

Discovery of Antibacterial Biotin Carboxylase Inhibitors by Virtual Screening and Fragment-Based Approaches

Igor Mochalkin^{†,*}, J. Richard Miller^{†,*,§}, Lakshmi Narasimhan^{†,§}, Venkataraman Thanabal^{†,‡}, Paul Erdman[¶], Philip B. Cox^{||}, J. V. N. Vara Prasad^{**}, Sandra Lightle^{††}, Michael D. Huband[‡], and C. Kendall Stover^{††,*}

Pfizer, Inc., Michigan Laboratories, Ann Arbor, Michigan 48105. [†]These authors contributed equally to this work. ^{*}Present address: Pfizer, Inc., Easter Point Road, Groton, Connecticut 06340. [§]Present address: Pfizer, Inc., 10777 Science Center Dr., San Diego, California 92121. [¶]Present address: Pfizer, Inc., Sandwich, U.K. ^{||}Present address: Abbott Laboratories, Abbott Park, Illinois 60064. ^{**}Present address: PTC Therapeutics, South Plainfield, New Jersey 07080. ^{††}Present address: Pfizer, Inc. Chesterfield, Missouri 63017. [‡]Present address: MedImmune LLC., Gaithersburg, Maryland 20878

The last few decades have seen a remarkable increase in bacterial resistance to the major classes of antibacterial agents (1, 2), rendering many of these classes useless or marginal for the therapy of serious bacterial infections. Despite the critical need for new antibiotics and significant advances in target validation and high-throughput screening technologies, there has not been a new antibiotic approved for human use in the postgenomic era, even though considerable pharmaceutical company resources have been applied to discovery efforts focused on generating new classes of antibiotics to novel bacterial targets. Most of these efforts have been largely based on whole-cell and cell-free target-based high-throughput screening strategies with very large synthetic or natural product compound libraries. One hypothesis explaining the lack of success for this antibacterial drug discovery paradigm is a lack of chemical diversity compatible with novel antibacterial targets, since most large pharmaceutical compound libraries are derived from efforts focusing on eukaryotic target space. In addition, it is believed that the physicochemical rules describing antibacterial compounds that can penetrate into the bacterial cytoplasm are considerably different from those commonly used for eukaryotic drug discovery (3, 4). While some antibiotic natural products may have been naturally selected to possess desirable antibacterial properties, they are also often very large molecules that do not possess other desirable drug-like properties and can be less tractable for medicinal chemistry lead optimization efforts.

ABSTRACT As part of our effort to inhibit bacterial fatty acid biosynthesis through the recently validated target biotin carboxylase, we employed a unique combination of two emergent lead discovery strategies. We used both *de novo* fragment-based drug discovery and virtual screening, which employs 3D shape and electrostatic property similarity searching. We screened a collection of unbiased low-molecular-weight molecules and identified a structurally diverse collection of weak-binding but ligand-efficient fragments as potential building blocks for biotin carboxylase ATP-competitive inhibitors. Through iterative cycles of structure-based drug design relying on successive fragment costructures, we improved the potency of the initial hits by up to 3000-fold while maintaining their ligand-efficiency and desirable physicochemical properties. In one example, hit-expansion efforts resulted in a series of amino-oxazoles with antibacterial activity. These results successfully demonstrate that virtual screening approaches can substantially augment fragment-based screening approaches to identify novel antibacterial agents.

*Corresponding authors,
Igor_Mochalkin@yahoo.com,
Richard.Miller2@pfizer.com,
StoverK@medimmune.com.

Received for review January 14, 2009
and accepted May 2, 2009.

Published online May 4, 2009

10.1021/cb9000102 CCC: \$40.75

© 2009 American Chemical Society

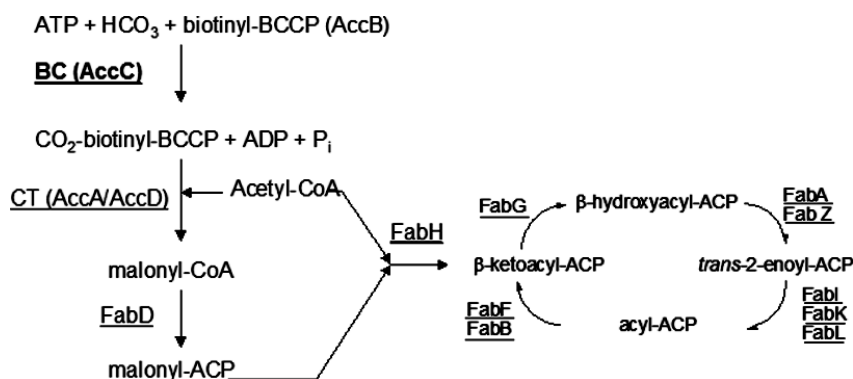


Figure 1. Type II fatty acid biosynthetic pathway. Gene products known to catalyze the indicated reactions in various bacterial species are underlined.

One possible paradigm to address these antibacterial discovery issues is fragment-based drug discovery, a potentially rapid, resource-efficient, and productive route to the identification of novel ligand-efficient hits in the early phase of the drug discovery process (5–11). This approach confers several potential advantages. Smaller compound fragments can feasibly probe a much greater proportion of the chemical space in the active site of the target protein (12–14) because they have a limited number of functional groups and, therefore, are less constrained in making higher-efficiency shape and electrostatic interactions with the protein binding site. Furthermore, through a process of structure-based fragment elaboration and growing, it is more possible to plan and build in desirable physicochemical properties while maintaining ligand efficiency in the process.

The type II fatty acid biosynthetic pathway (Figure 1) has long been considered an excellent target for antibacterial drug discovery, and considerable *in vitro* and *in vivo* data from multiple organisms, enzyme targets, and inhibitors support this hypothesis (15–17). We have previously described potent biotin carboxylase (BC) inhibitors identified by whole-cell screening (18). Bacterial acetyl-CoA carboxylase (ACCase) is a multifunctional biotin-dependent enzyme that consists of three separate proteins: BC, BC carrier protein (BCCP), and carboxyltransferase (CT) (19). In the first half-reaction, BC catalyzes the ATP-dependent transfer of the

carboxyl group from bicarbonate to biotin of BCCP (Figure 1). In the second half-reaction, the carboxyl group is transferred from carboxybiotinylated BCCP to acetyl-CoA to produce malonyl-CoA. Because BC catalyzes the first committed step in fatty acid biosynthesis, is amenable to sensitive high-throughput enzymatic assays (18, 20), and is structurally tractable for crystallographic studies, we selected BC as a candidate for a fragment-based discovery approach. Herein, we present two complementary fragment-based approaches designed to identify and advance novel classes of BC inhibitors. The first approach included ligand-based virtual screening (VS) using

3D shape similarity searching coupled with a high-concentration ACCase biochemical assay to validate the VS hits (Supplementary Figure 1a). The starting point for this screening approach was the previously described pyridopyrimidine BC inhibitor **1** (Figure 2), which has a binding affinity of 5 nM for the *Escherichia coli* BC (*EcBC*) enzyme, high-resolution X-ray crystal structure (PDB accession code 2v58), and *in vitro* and *in vivo* antibacterial activity (18). The second approach consisted of using the high-concentration biochemical assay to screen a large library of proprietary molecular frag-

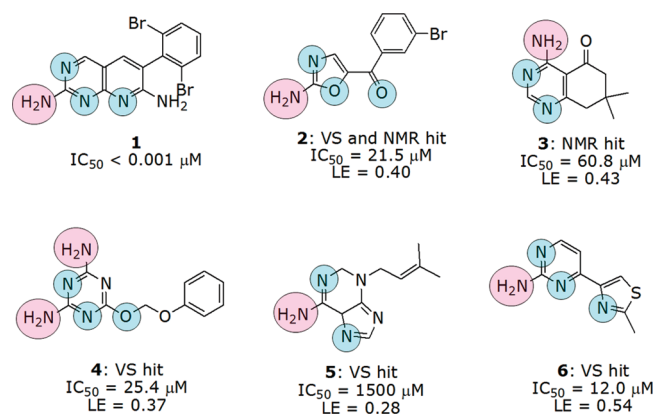


Figure 2. Chemical structures and selected pharmacophore features of pyridopyrimidine inhibitor **1** and various VS and NMR fragment hits. Pharmacophore features are shown in the following colors: hydrogen bond acceptors are in cyan; hydrogen bond donors are in pink. Ligand efficiency (LE) (42) was used for selection of the hits. Because LE is equal to the free energy of binding of a ligand to a receptor binding site averaged for each non-hydrogen atom, LE prioritizes hits by the averaged binding efficiency of individual ligand atoms and not the absolute value of potency alone.

ments and scaffolds followed by saturation transfer difference NMR (STD-NMR) methods to confirm inhibitor binding to BC (Supplementary Figure 1b). Both approaches produced several ligand-efficient fragment hits with different chemotypes (Figure 2). The structures of fragment molecules bound to the enzyme provided profound insights into the nature of the fragment–protein interactions and enabled effective fragment-to-lead optimization by medicinal chemistry. Several strategies were used to improve upon the potency of fragment hits **2**, **3**, and **6**. In one example, a fragment hit produced a novel series of BC inhibitors with mechanism-based antibacterial activity. In addition to describing several series of novel BC inhibitors derived from fragment and virtual screening approaches, our work provides templates for the utilization of computational or experimental fragment-based methods in drug discovery that can be applied to other therapeutic targets.

RESULTS AND DISCUSSION

Identification of BC Inhibitors by Virtual Screening.

The availability of the crystal structure of *Ec*BC in complex with **1** enabled efficient VS guided by 3D shape and electrostatics surface similarity searching using the ROCS and EON software programs (21), followed by empirical scoring of the generated hits at the *Ec*BC active site and subsequent visual inspection to accept or reject the proposed binding modes. A total of 525 compounds from a virtual screen of 2.2 million compounds (Supplementary Figure 1a) were selected for testing in the previously referenced ACCase biochemical assay (18) at a concentration of 30 μ M. Of these compounds, 9% (48 of tested VS hits) had IC_{50} values less than 10 μ M. The enrichment provided by this approach was remarkable because the hit rate of the virtual screening was approximately 200-fold higher than that achieved in a traditional HTS screen that utilized the same enzyme assay (data not shown).

Identification of BC Inhibitors by Fragment

Screening. A library of 5200 fragments was screened in pools of 10 compounds per well at the concentrations of 98 and 238 μ M of each compound (Supplementary Figure 1b). Screening was performed using the enzyme-coupled ACCase assay (18). In this screen, 96 fragment pools exhibited greater than 25% inhibition at one or both concentrations. Deconvolution of these pools by STD-NMR assessment of BC binding resulted in 142 hit

compounds. These hits were then individually titrated in the ACCase enzyme assay, and six fragments were found to have IC_{50} values less than 95 μ M. Several selected hits with ligand efficiencies ranging from 0.54 to 0.28 are shown (Figure 2).

Fragment Hits Share Similar Pharmacophore

Features. Based on superposition of 2D chemical structures, the identified fragment hits shared pharmacophore features known to be important for binding to the BC ATP-binding site (22). All fragment hits had combinations of hydrogen-bond donors and acceptors that are important for interaction with the hinge region of the enzyme (Figure 2). Noticeably, fragment **2** contained an amine group in the oxazole ring (five-membered heterocyclic ring system), analogous to the amine in the pyrimidine ring (six-membered heterocyclic ring system) of compound **1** and fragment **6**. It was interesting to note that while the fragment **3** amine functionality was in a different position compared with those of compound **1** or fragments **2**, **5**, and **6**, the fragment **4** amine groups were at both positions. Fragment **4** also showed that the oxygen atom in the side chain could be used to make a hydrogen bond, thereby serving an analogous role to the pyridine nitrogen of inhibitor **1** or the carbonyl oxygen atom of fragment **2** (Figure 2). While all these compound fragments were considered potentially tractable for synthetic elaboration, fragments **4** and **5** were deprioritized as less synthetically attractive than fragments **2** and **3**.

Characterization of Fragment Binding Modes. To enable effective fragment-based lead optimization, the binding modes of fragments were characterized using X-ray crystallography to gain insights into the nature of the protein–fragment interactions to guide structure-based compound design strategies. Briefly, the ATP-binding region of BC can be arbitrarily divided into three distinct sites: (1) adenine-binding site, (2) ribose-binding site, and (3) phosphate-binding site (22). The adenine-binding region consists of the Glu201–Leu204 and Ile157–Lys159 structural segments that encircle the plane of adenine and residues Leu278 and Ile287 positioned above and below the plane of the base. Adjacent to the adenine-binding site, the ribose-binding region is formed by the side chains of residues His209, Gln233, His236, Ile437, and His438 positioned to accommodate the ribose group of the nucleotide. The binding of inhibitor **1** induces conformational changes in the ribose-binding region to produce a hydrophobic

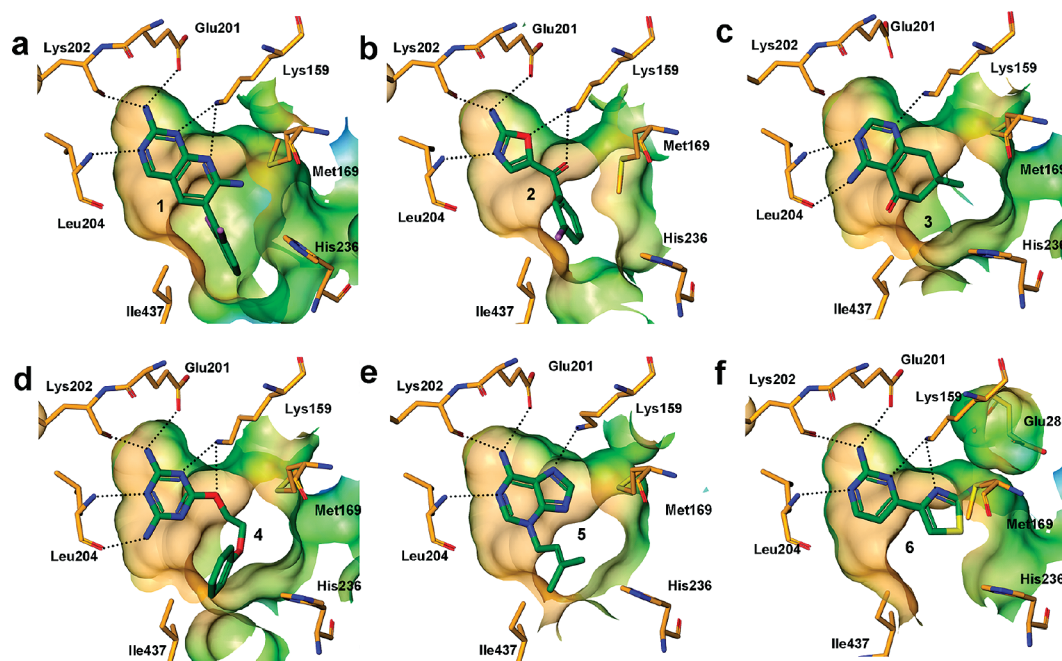


Figure 3. Binding modes of compound 1 and fragments 2–6 to the ATP-binding site of *EcBC* determined by X-ray crystallography. The ligand molecules and protein residues are shown as sticks and colored in the following atom colors: carbon (ligands), green; carbon (protein), orange; nitrogen, blue; oxygen, red; and sulfur, yellow. Connolly binding-site surfaces of BC were calculated using the fragment-bound crystal structures and colored by hydrophobicity (hydrophobic areas are in brown and hydrophilic areas are in blue and red). a) View of the binding mode of inhibitor 1. b) View of the binding mode of fragment 2. c) View of the binding mode of fragment 3. d) View of the binding mode of fragment 4. e) View of the binding mode of fragment 5. f) View of the binding mode of fragment 6a.

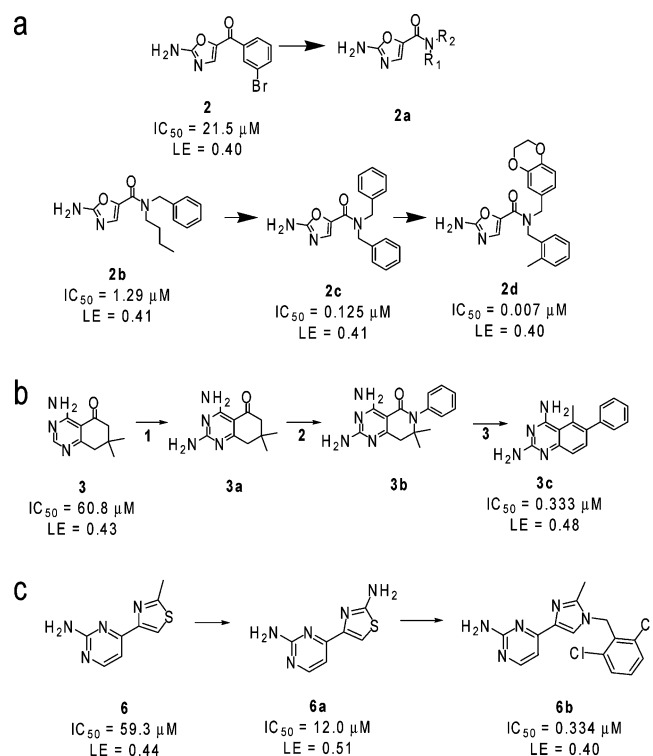
subpocket that encloses the dibromo-benzyl group of the inhibitor. Hereinafter, this subpocket is referred to as a hydrophobic enclosure. The phosphate-binding site includes residues Lys116, Lys159, and the glycine-rich loop (residues 161–168) that coordinate the phosphate groups of the substrate. BC from *E. coli* and *Pseudomonas aeruginosa* can be readily crystallized with inhibitors using crystallization conditions described elsewhere (18, 22, 23), yielding high-resolution complex crystal structures. Calculated electron density OMIT maps (Supporting Figure 2) were used to unambiguously identify ligands bound to the BC active site. Analysis of the crystal structures indicated that the molecular fragments bind to the adenine-binding region of the BC active site (Figure 3a–f). Structure superposition of *EcBC* in complex with fragments 2–6 indicated that the side chains of all key residues in the adenine-binding region are optimally positioned for binding of the fragments and remain in the same conformation

upon binding. This lack of backbone and side chain motion provided confidence that docking methods could accurately predict binding modes of fragments and lead compounds during fragment-to-lead optimization. In particular, docking compounds using the *GOLD* (24) or *Glide* (25) software packages was effective in reproducing the fragment binding modes observed in X-ray crystal structures and was used extensively to select new compounds for synthesis and structure–activity relationship development.

Fragment-to-Lead Optimization. To develop alternate inhibitor series in the event

that one or more primary series fail due to other reasons (*e.g.*, poor *in vivo* efficacy), we enabled fragment-to-lead optimization approaches including fragment growing, merging, and morphing. The fragment linking approach was not applicable because all the identified fragments interacted with the adenine-binding region of BC. An effective fragment optimization strategy was achieved through iterative cycles of (1) library design (Supporting Information) and modeling-driven evaluation of virtual libraries for synthesis, (2) parallel medicinal chemistry synthesis (Supporting Information), (3) screening of newly synthesized compounds in the AC-Case bioassay to determine binding affinities, and (4) cocrystal structure determination of selected leads to explore ligand–protein interactions and the solvent network structure. The results of optimization for the selected fragment hits are summarized.

Optimization of Fragments 2 and 3 by Fragment Growing. Fragment growing was accomplished by assessing and exploiting the neighboring ribose-binding

SCHEME 1. Fragment-to-lead optimization^a

^aa) Evolution of fragment **2** into lead compound **2d** through fragment modification to amide **2a** to achieve synthetic feasibility, fragment growing into the BC hydrophobic enclosure formed by the active-site residues Ile437, His209, Leu278, and His236 to achieve potency, and final optimization of the side-chain groups of inhibitors. b) Evolution of fragment **3** into lead compound **3c** achieved by (1) establishing a hydrogen-bond interaction with the side-chain oxygen atoms of residue Glu201, (2) growing fragment **3a** into the hydrophobic enclosure formed by residues Ile437, His209, Leu278, and His236 of BC, and (3) morphing the dihydropyridopyrimidinone into the quinazoline core. c) Evolution of fragment **6** into lead compound **6b** achieved by merging ligand-efficient scaffold **6a** with the dichlorobenzyl group of pyridopyrimidine inhibitors of BC.

site, which includes the hydrophobic enclosure, using parallel medicinal chemistry. The design of novel compounds was driven by two criteria: (1) the drug-likeness of the compounds characterized by the molecular physicochemical properties and (2) similarity of the compound binding mode to that of inhibitor **1**. In library design, we omitted monomers with multiple reactive centers, and selected only those final compounds that had molecular weight below 350 Da and complied with the empirical Lipinski's rule-of-five (26). Our previous observation that the hydrophobic enclosure formed by residues Ile437, His209, Leu278, and His236 contributed significantly to the potency of pyridopyrimidine BC inhibitors (18), including compound **1**, was pivotal in guiding new design. Indeed, extending fragments **2** and **3** into the BC hydrophobic enclosure confirmed that it

was possible to increase potency without compromising their ligand efficiency (Scheme 1, panel a, and Figure 4, panels a–c; Scheme 1, panel b, and Figure 4, panels d–f). Considering synthetic feasibility, we reasoned that amino-oxazole fragment **2** ($IC_{50} = 21.5 \mu M$, $LE = 0.40$) could be more readily analogued as the corresponding amides **2a** (Scheme 1, panel a). These analogues were accessible from the commercially available 2-amino-1,3-oxazole carboxylic acid ester *via* amidolysis after straightforward saponification of the ester (Scheme 2). In the first successful synthetic iteration, the amide **2b** was identified (Supporting Information). Compound **2b** exhibited a 20-fold boost in potency over the starting fragment **2**. A second iteration led to the dibenzylamide **2c** with a net 200-fold potency boost over the starting fragment. A BC cocrystal structure of

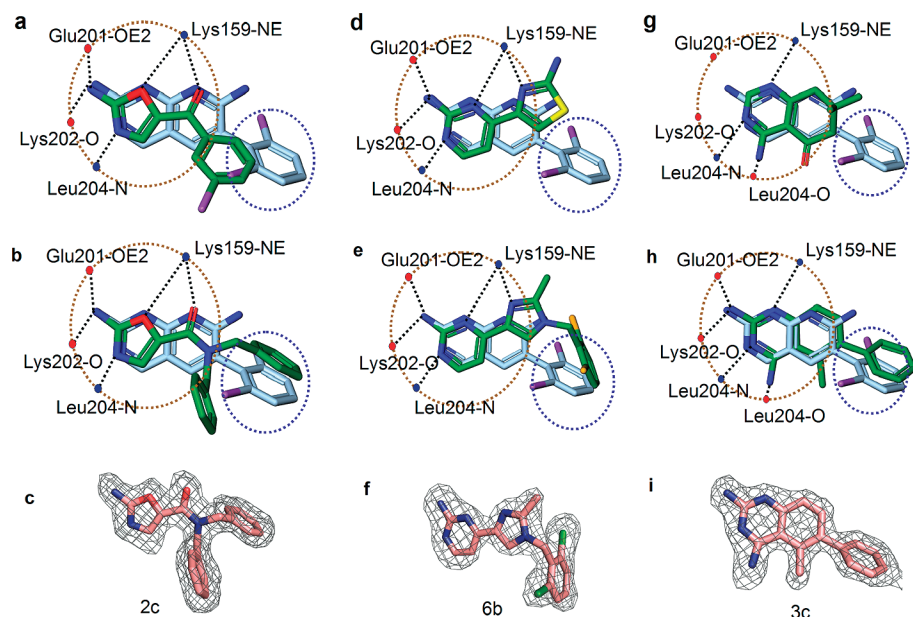


Figure 4. Optimization of fragments 2, 3, and 6 *via* growing, morphing, and merging. **a)** View of superimposed inhibitor 1 and initial fragment 2. Hydrogen-bonding interactions between 2 and BC are highlighted. **b)** View of superimposed inhibitor 1 and lead compound 2c that accesses the hydrophobic enclosure and exhibits 200-fold boost in potency over the initial fragment hit 2. **c)** View of the ($F_o - F_c$) OMIT electron density map of compound 2c calculated by omitting the ligands during simulated annealing. Map is contoured at 2.0σ level and then superimposed with the final refined model. **d)** View of superimposed inhibitor 1 and initial fragment 3. Hydrogen-bonding interactions between 3 and BC are highlighted. **e)** View of superimposed inhibitor 1 and lead compound 3c. **f)** View of the ($F_o - F_c$) OMIT electron density map of compound 3c calculated by omitting the ligands during simulated annealing. Map is contoured at 2.0σ level and then superimposed with the final refined model. **g)** View of superimposed inhibitor 1 and initial fragment 6a. Hydrogen-bonding interactions between 6a and BC are highlighted. **h)** View of superimposed inhibitor 1 and fragment 6b that accesses the hydrophobic pocket of the BC active site and exhibits 35-fold potency increase over the initial hit. **i)** View of the ($F_o - F_c$) OMIT electron density map of compound 6b calculated by omitting the ligands during simulated annealing. Map is contoured at 2.0σ level and then superimposed with the final refined model.”

this fragment revealed edge-to-face interactions of the ligand with the protein, which was subsequently optimized in the next iteration by selecting more electron-rich dibenzylamines. This led to the identification of amino-oxazole **2d** ($IC_{50} = 0.007 \mu M$, LE = 0.40) with a

net 3000-fold boost in potency over the original fragment **2**. Compounds **2c**, **2d**, and related analogues define a novel lead series with *in vitro* antibacterial activity as discussed below. Protocols describing the synthesis of amino-oxazole compounds **2b**, **2c**, and **2d** are provided in Supporting Information.

Optimization of Fragment 6 by

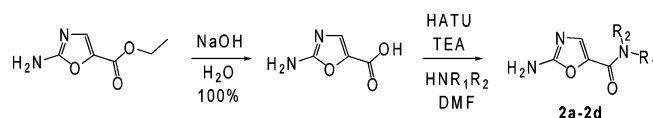
Merging. Fragment merging involves combining structural information at the level of functional groups of the superimposed series of compounds and fragments to generate a potent lead compound (27). It is also referred to as “mixing and matching” of functional groups from different fragments and compound series. As an example of fragment optimization by merging, the ligand-efficient amino-pyrimidine scaffold of fragment **6a** was merged with the 2,6-dichlorobenzyl group similar to that of inhibitor **1** via the imidazole linker (Scheme 1, panel c, and Figure 4, panels g–i). With an addition of dichlorobenzyl, the binding affinity increased more than 35-fold from $12.0 \mu M$ to 334 nM , while maintaining a ligand efficiency of 0.40 and preserving the same protein–ligand binding mode.

Improving Ligand Diversity by

Fragment Morphing. In addition to fragment growing and merging, improved ligand diversity and properties

can be achieved using fragment morphing techniques. To identify unexplored chemical space for a new chemotype, the BC fragments and inhibitor **1** were used as starting structures to define reasonable structural transformations of fragments into new compounds. Struc-

SCHEME 2. Preparation of amino-oxazole amides **2a–2d** *via* standard chemistry starting from 2-amino-1,3-oxazole carboxylic acid ester



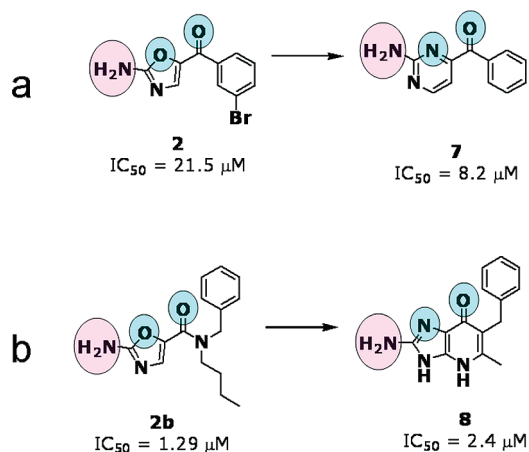


Figure 5. Structural diversity of fragment hits can be enriched using fragment morphing. a) Structural transformation of fragment 2 (five-membered heterocyclic ring system) to fragment 7 (six-membered heterocyclic ring system). b) Structural transformation of fragment 2b to fragment 8.

tural mutations, such as atom type exchange, atom addition and removal, bond saturation, unsaturation, and rearrangement (28, 29) were used to generate a set of new molecules. Evolution of amino pyrimidine ketone fragment 3 ($IC_{50} = 60.8 \mu M$, LE = 0.43) was iterated into a more potent analogue 3c through fragment morphing and growing (Scheme 1, panel b, and Figure 4, panels d–f). First, the functional amine group was introduced to the compound to establish a hydrogen bond with the side chain of Glu201. Second, the bicyclic ring

system was aromatized to introduce a benzyl group into the hydrophobic pocket to gain potency. Moreover, the amino-oxazole (five-membered ring) of fragment 2 (Figure 5, panel a) was morphed into the amino-pyrimidine (six-membered ring) of fragment 7 by atom/bond addition guided by the pharmacophore features important for the interactions with the enzyme, while the amino-oxazole carboxamide core group of fragment 2b (Figure 5, panel b) was transformed into the amino-imidazo-pyridinone core of fragment 8 by cyclization. Several compounds containing these novel scaffolds were identified in our proprietary compound collection, docked into the BC active site, and tested in the biochemical assay. While the biochemical assay indicated that no significant improvement in potency was achieved (Figure 5, panels a and b), the desired outcome of fragment morphing improved structural diversity delivering a wider range of physicochemical properties, synthetic attractiveness, and tractability of the compounds.

Antibacterial Activity of Amino-oxazoles Is Due to Inhibition of Biotin Carboxylase. During optimization of the amino-oxazole fragment hits (Scheme 1, panel a), we observed that the most potent BC inhibitors 2c and 2d exhibited antibacterial activity against fastidious Gram-negative pathogens and efflux-pump-deficient *E. coli*, a spectrum of antibacterial activity similar to the pyridopyrimidine BC inhibitors (typified by compound 1, Table 1). To confirm that the antibacterial activity of 2c was due to inhibition of BC, this compound was ex-

TABLE 1. Minimal inhibitory concentrations (MIC, $\mu g mL^{-1}$) values of the BC inhibitors

Strain (genotype) ^a , additives	1	2c	2d	Linezolid
<i>E. coli</i> (tolC, imp [−])	0.125	16	8	8
<i>E. coli</i> (tolC, imp [−]), 2% HSA ^b	0.5	32	32	8
<i>E. coli</i> (wild-type)	16	>64	>64	>64
<i>H. influenzae</i> (acrA)	0.125	4	4	8
<i>H. influenzae</i> (acrA, I437T BC)	16	64	64	8
<i>H. influenzae</i> (wild-type)	0.125	>64	>64	16
<i>Moraxella catarrhalis</i> (acrA)	0.5	4	8	8
<i>M. catarrhalis</i> (wild-type)	1	8	16	8
<i>Pseudomonas aeruginosa</i> (mexAB oprM)	32	>64	>64	64

^aThe following designate targeted knockouts of efflux pumps or subunits of efflux pumps: tolC, acrA, norA, mexAB, oprM. The imp gene disruption further sensitizes *E. coli* to inhibitors. The accC-I437T genotype in *Haemophilus* results from spontaneously resistant mutants selected in the presence of compound 1. ^bHSA is human serum albumin.

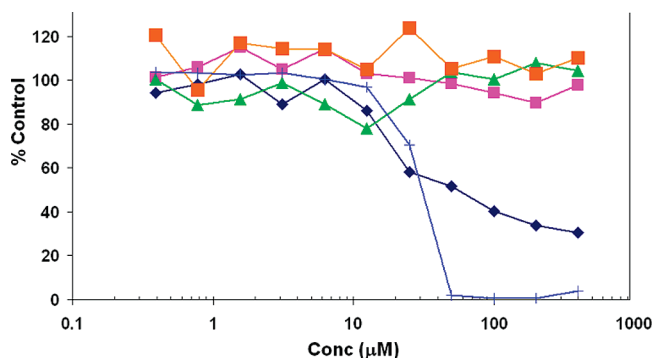


Figure 6. Effect of various concentrations of **2c** on *E. coli* macromolecular synthesis. Mid-log phase *E. coli* cells were exposed to the indicated concentrations of compound **2c** and radiolabeled precursors of DNA (thymidine), RNA (uridine), protein (leucine), and fatty acids (acetate) as previously described (18). Incorporation of label relative to untreated cells, as well as a compound-treated cell growth control, are shown. Graph symbols are pink squares = protein, orange squares = RNA, green triangles = DNA, blue plus signs = cell growth, and dark blue diamonds = fatty acids.

aminated in an *E. coli* macromolecular biosynthesis assay monitoring RNA, DNA, protein, and fatty acid biosynthesis (18). Compound **2c** specifically inhibits biosynthesis of fatty acids at concentrations consistent with those that inhibit bacterial growth (Figure 6). Although **2d** exhibits a nearly 20-fold improvement in potency against the BC enzyme, this does not translate into improved antibacterial activity. This observation highlights one of the major challenges of antibacterial drug discovery, the frequent lack of correlation between enzyme target potency and whole-cell activity. Since **2d** and **2c** show similar loss in potency between efflux-proficient and -deficient strains of *Haemophilus influenzae*, differences in antibacterial activity cannot be attributed to differences in susceptibility to efflux by the *acrA* efflux pump. A more likely explanation is a difference in cellular penetration, target dissociation rate, or both.

Further support for BC inhibition as the mechanism of **2c** and **2d** action is the reduction of antibacterial activity against strains containing BC with an I437T mutation, which confers resistance to pyridopyrimidines such as **1** (18). It is important to note that the effects of the I437T mutation on the antibacterial activity of **2c** and **2d** (16-fold) is considerably less than that observed for pyridopyrimidine **1** (128-fold, Table 1). This argues that the amino-oxazoles could offer insights into avoidance of spontaneous resistance to BC inhibitors.

While fatty acid biosynthesis has long been considered an excellent target for antibacterial drug discovery (1, 15, 17), a recent report has called into question the utility of inhibitors for treatment of Gram-positive infections based on data from *Streptococcus agalactiae* (30). Brinster *et al.* (30) presented data indicating that *de novo* fatty acid biosynthesis is not essential for *S. agalactiae* virulence and, therefore, fatty acid biosynthesis inhibitors are unlikely to be efficacious *in vivo* against this organism. However, these observations do not necessarily translate to Gram-negative organisms described here and may not apply to all Gram-positive organisms (31). Additional *in vitro* and *in vivo* studies must be undertaken before antibacterials targeting fatty acid biosynthesis are discounted as viable therapeutic agents.

Amino-oxazoles Are Selective Inhibitors of Bacterial Biotin Carboxylase. As has been previously noted, the bacterial BC possesses structural similarity to eukaryotic protein kinases and the human orthologue (18). To confirm the bacterial selectivity of the amino-oxazoles, compound **2c** was tested against a panel of over 40 different human protein kinases (18), as well as the rat liver acetyl-CoA carboxylase. In all cases, the IC_{50} of compound **2c** was $>10,000$ nM (data not shown).

Conclusion. Effective NMR and bioassay experimental screening techniques and computational methods of fragment screening were designed and optimized for the bacterial biotin carboxylase enzyme. The screening methods produced a rich collection of molecular fragments and starting chemical lead matter that were characterized by X-ray crystallography, highly enabling the optimization process.

The fragment hits were effectively optimized into multiple novel lead series using concepts of fragment growing, merging, and morphing. Because of the general nature of fragment screening and optimization, the methods and strategies we discuss are applicable to other enzyme or protein therapeutic targets.

The new series of fragment-derived BC inhibitors possessed antibacterial activity due to inhibition of the target enzyme and could serve as leads for the development of potent new antibacterial therapies.

METHODS

Generation of Protein Reagent. Cloning, expression, and purification protocols of EcBC were previously described elsewhere (22) and are available in the Supporting Information. The purified protein was stored at -80°C in the buffer consisting of 10 mM HEPES, pH 7.2, 250 mM KCl, and 1 mM tris(2-carboxyethyl) phosphine hydrochloride (TCEP).

Preparation of a Database for Virtual Screening. A subset of the Pfizer database of small organic molecules used in virtual screening by ROCS and EON (OpenEye Scientific Software Inc.) was prepared using the following preparation steps: (1) remove compounds containing metals, incorrect atomic valency, and re-

active functional groups using protocols implemented in the Pipeline Pilot software (Accelrys Software, Inc.); (2) select compounds with a minimum ring size of five; (3) select compounds with a combined nitrogen and oxygen atom count equal or greater than two; (4) select compounds with the number of rotatable bonds less than 12; (5) select compounds with the molecular weight value between 150 and 600 Da; (6) remove any structural duplicates; (7) validate compound stereochemistry. Those compounds that contain one or two unknown stereocenters were enumerated for all possible stereoassignments. For those compounds that contain more than two undefined stereocenters, the stereocenters were assigned randomly.

TABLE 2. X-ray intensity data collection and refinement statistics of deviations from ideality and final refinement parameters and the final R and R -free values

	2	2c	3	3c	4	5	6a	6b
PDB deposition	2w6m	2w6n	2w6o	2w6p	2w6q	2w6z	2w70	2w71
Data collection								
Space group	$P2_12_12_1$	$P2_12_12_1$	$P2_12_12_1$	$P2_12_12_1$	$P2_12_12_1$	$P2_12_12_1$	$P2_12_12_1$	$P2_12_12_1$
Cell dimensions								
a, b, c (Å)	84.24, 106.20, 122.28	84.14, 105.94, 122.45	68.63, 113.37, 121.74	83.986, 106.475, 121.978	84.00, 105.57, 122.05	84.48, 106.90, 122.41	84.23, 106.21, 122.63	80.66, 113.74, 121.79
α, β, γ (deg)	90.0, 90.0, 90.0	90.0, 90.0, 90.0	90.0, 90.0, 90.0	90.0, 90.0, 90.0	90.0, 90.0, 90.0	90.0, 90.0, 90.0	90.0, 90.0, 90.0	90.0, 90.0, 90.0
Resolution (Å) ^a	2.0 (2.07–2.0)	1.87 (1.94–1.87)	2.5 (2.59–2.50)	1.85 (1.92–1.85)	2.05 (2.12–2.05)	1.90 (1.97–1.90)	1.77 (1.83–1.77)	1.99 (2.06–1.99)
R_{merge}^a	0.083 (0.505)	0.050 (0.318)	0.102 (0.467)	0.056 (0.487)	0.082 (0.499)	0.057 (0.354)	0.076 (0.540)	0.061 (0.544)
$I/(\sigma I)$	25.23 (4.47)	39.97 (5.33)	14.45 (2.93)	24.17 (2.71)	16.22 (2.5)	29.58 (4.76)	20.54 (2.35)	23.34 (2.63)
Observations ^a	510187 (49265)	494896 (17852)	138321 (11358)	379942 (34135)	264822 (25692)	395276 (39368)	529379 (49707)	339096 (30246)
Unique reflections ^a	74778 (7353)	86865 (6156)	29998 (2989)	89788 (8983)	66405 (6423)	67879 (7030)	107085 (10576)	75853 (7034)
Completeness (%)	99.9 (99.7)	95.2 (68.2)	88.4 (90.0)	95.5 (96.9)	96.9 (94.9)	77.4 (81.2)	99.9 (99.9)	98.1 (92.1)
Redundancy	6.82 (6.7)	5.7 (2.9)	4.61 (3.8)	4.23 (3.8)	3.99 (4.0)	5.82 (5.6)	4.94 (4.7)	4.47 (4.3)
Refinement								
R_{work}^b	0.1834	0.1753	0.2298	0.1869	0.1840	0.1847	0.1745	0.1935
R_{free}^c (5% data)	0.2078	0.2166	0.3080	0.2163	0.2245	0.2195	0.2023	0.2293
No. atoms								
Protein (chains A/B)	3449/3447	3425/3425	3425/3433	3433/3005	3449/3447	3449/3447	3444/3450	3440/3434
Ligand/ion	15/15	23/23	14/14	19/0	18/18	15/0	13/13	22/22
Water	810	1062	129	726	701	510	942	672
B -factors								
Protein (chains A/B)	21.53/ 26.97	19.06/ 22.97	31.00/ 34.78	21.92/ 21.07	24.32/ 29.04	20.81/ 30.90	21.77/ 25.68	25.55/ 29.46
Ligand	25.0/ 59.0	19.2/ 30.6	39.5/ 50.1	23.30	34.5/ 48.5	22.6	23.3/ 36.8	34.3/ 47.5
Water	29.53	33.67	25.93	31.73	31.65	28.48	31.15	34.13
RMS deviations								
Bond lengths (Å)	0.007	0.009	0.009	0.008	0.008	0.007	0.008	0.008
Bond angles (deg)	0.995	1.224	1.132	1.081	1.057	1.109	1.118	1.942
Ramachandran plot statistics ^d								
Most favored region	707 (93.0)	705 (92.8)	692 (91.1)	654 (92.0)	702 (92.4)	698 (91.8)	701 (92.2)	703 (92.5)
Allowed region	50 (6.6)	52 (6.8)	65 (8.6)	54 (7.6)	54 (7.1)	58 (7.6)	56 (7.4)	55 (7.2)
Generously allowed region	1 (0.1)	1 (0.1)	1 (0.1)	1 (0.1)	2 (0.3)	2 (0.3)	1 (0.1)	0
Disallowed region	2 (0.3)	2 (0.3)	2 (0.3)	2 (0.3)	2 (0.3)	2 (0.3)	2 (0.3)	2 (0.3)

^aNumbers in parentheses indicate statistics for the high-resolution data bin. ^b $R_{\text{merge}} = \sum hkl \sum i (|hkl_i| - \langle |hkl| \rangle) / \sum hkl \sum i |hkl_i|$. ^c $R_{\text{work}} = \sum hkl |F_o(hkl) - F_c(hkl)| / \sum hkl |F_o(hkl)|$, where F_o and F_c are observed and calculated structure factors, respectively. ^dNumbers in parentheses indicate percent of total non-glycine and non-proline residues.

Preparation of a NMR Fragment Library. The NMR fragment library was assembled from compounds available in the Pfizer proprietary compound collection or ordered from various commercial sources (Supporting Information) using the following molecular property filters: (1) molecular weight ($150 \text{ Da} \leq \text{MW} \leq 300 \text{ Da}$); (2) lipophilicity ($\text{clogP} \leq 3$); (3) number of hydrogen bond donors ($\text{HBD} > 1$), and (4) number of hydrogen bond acceptors ($\text{HBA} \leq 3$). The final library contained 70% molecules with two or more functional groups that can enable a rapid hit-to-lead optimization by medicinal chemistry. The library was characterized by proton NMR (^1H NMR) spectroscopy to ensure aqueous solubility and compound structural integrity.

ACCCase Coupled Enzyme Assay. An enzyme-coupled phosphate detection assay was utilized to assess potency of the compounds as described elsewhere (18). Inhibition data were fit to the standard IC_{50} equation.

$$\frac{v_i}{v_0} = \frac{1}{1 + ([I]/\text{IC}_{50})^n} \quad (1)$$

where v_i is the reaction velocity at a given concentration of inhibitor $[I]$, v_0 is the uninhibited velocity, and n is the Hill slope. For potent compound **2d** ($\text{IC}_{50} = 7 \text{ nM}$), the data were fit using the Morrison equation (32)

$$v_i = v_0 \left(\frac{([E]_T - [I]_T - K_i^{\text{app}}) + \sqrt{([E]_T - [I]_T - K_i^{\text{app}})^2 + 4K_i^{\text{app}}[E]_T}}{2[E]_T} \right) \quad (2)$$

where v_i is the reaction velocity at a given concentration of inhibitor, v_0 is the uninhibited velocity, $[E]_T$ is the concentration of enzyme, K_i^{app} is the apparent inhibition constant, and $[I]_T$ is the inhibitor concentration.

Fragment Screening by NMR. NMR samples contained $2 \mu\text{M}$ of EcBC and a screening library pool of 10 compounds, each at a concentration of $200 \mu\text{M}$, in $500 \mu\text{L}$ of 10 mM deuterated HEPES buffer, 2 mM DTT, 10 mM KCl, at $\text{pH} = 7$. ^1H NMR data were collected on a Bruker Avance 600 MHz spectrometer equipped with a 5 mm TXI cryo-probe and an autosampler. NMR screening experiments were carried out at 298 K utilizing saturation transfer difference (33) with on-resonance irradiation at 0 ppm and off-resonance irradiation at -5 ppm (34). The difference spectra were generated from on- and off-resonance data collected in an interleaved fashion. Excitation sculpting was used for water suppression (35). Typically 512 scans with 16 dummy scans were collected per data set. Deconvolution of the STD-NMR spectra from the pools into individual compound hits were carried out using an in-house software package.

Crystallographic Characterization of Compounds in Complex with *E. coli* BC. To prepare protein–fragment complexes, a 100 mM stock solution of each fragment was dissolved in dimethyl sulfoxide and mixed with the protein (12 mg mL^{-1}) to a final fragment concentration of 5.0 mM . The complex was incubated at 4°C for 4 h before crystallization. The crystals were grown at ambient temperature using the hanging-drop vapor diffusion method. Four microliter drops consisted of equal parts of the protein solution containing each fragment and the reservoir solution composed of 0.1 M KCl and $2\text{--}8\%$ PEG-800. X-ray diffraction data from the crystals were collected in-house or at the Advanced Photon Source facility on beamline 17-ID operated by the Industrial Macromolecular Crystallography Association

(Table 2). The crystals were mounted in the cryo-loops and treated with the cryo-protection solutions consisting of 4 parts of crystallization well solution and 1 part of ethylene glycol. The final concentration of ethylene glycol in the cryo-protecting solution was $20\text{--}25\%$. The crystals were moved from the crystallization drop to cryo-solution for $3\text{--}5 \text{ s}$ before being flash-frozen in liquid nitrogen. Intensity data were measured at about -180°C . One X-ray data set was collected for each crystal. Autoindexing and processing of the measured intensity data were carried out with the HKL2000 software package (36). The intensity data-collection statistics are summarized in Table 2. The crystal structures were solved by molecular replacement using the coordinates of EcBC as the search model (PDB code 2j9g). The rotation/translation searches were carried out with the MOLREP program (37). The molecular replacement solution was further optimized by rigid-body, coordinates, and B -value minimization using the CNX 2000 (38) (Accelrys Software Inc.) or REFMAC (39) software programs. Calculated $(2F_o - F_c)$ and $(F_o - F_c)$ electron density maps were utilized for interactive fitting of protein structures and ligands into electron density using the COOT software program (40). Protein model building was alternated with coordinate minimization and individual B -factor refinement using REFMAC (39). Final coordinates were validated using the PROCHECK validation tools (41). Summary of final refinement parameters and the final R -work and R -free values are listed in Table 2.

Coordinates and accession codes.

Acknowledgment: The authors would like to acknowledge the following Pfizer colleagues: A. Choy, J. Y. Kim, C. Manning, K. Skinner, and T. McQuade for their considerable technical contributions and scientific advice; J. Withka and T. V. Magee for critical review of the manuscript and suggestions. We also acknowledge the advice and encouragement of Dr. G. Waldrop, Louisiana State University, Baton Rouge, LA. The authors declare they have no competing interests.

Supporting Information Available: This material is available free of charge via the Internet at <http://pubs.acs.org>.

Accession Codes: Atomic coordinates of the reported fragments and the related compounds in complex with *E. coli* BC are deposited in the RCSB Protein Data Bank: 2w6m (fragment **2**), 2w6n (compound **2c**), 2w6o (fragment **3**), 2w6p (compound **3c**), 2w6q (fragment **4**), 2w6z (fragment **5**), 2w70 (fragment **6a**), and 2w71 (compound **6b**).

REFERENCES

- Payne, D., and Tomasz, A. (2004) The challenge of antibiotic resistant bacterial pathogens: the medical need, the market and prospects for new antimicrobial agents, *Curr. Opin. Microbiol.* **7**, 435–438.
- Alanis Alfonso, J. (2005) Resistance to antibiotics: are we in the post-antibiotic era? *Arch. Med. Res.* **36**, 697–705.
- Silver, L. L. (2008) Are natural products still the best source for antibacterial discovery? The bacterial entry factor, *Expert Opin. Drug Discovery* **3**, 487–500.
- O'Shea, R., and Moser, H. E. (2008) Physicochemical properties of antibacterial compounds: implications for drug discovery, *J. Med. Chem.* **51**, 2871–2878.
- Congreve, M., Chessari, G., Tisi, D., and Woodhead, A. J. (2008) Recent developments in fragment-based drug discovery, *J. Med. Chem.* **51**, 3661–3680.
- Erlanson, D. A., McDowell, R. S., and O'Brien, T. (2004) Fragment-based drug discovery, *J. Med. Chem.* **47**, 3463–3482.
- Fattori, D. (2004) Molecular recognition: the fragment approach in lead generation, *Drug Discovery Today* **9**, 229–238.

8. Hajduk, P. J., and Greer, J. (2007) A decade of fragment-based drug design: strategic advances and lessons learned, *Nat. Rev. Drug Discovery* 6, 211–219.
9. Nienaber, V. L., Richardson, P. L., Klighofer, V., Bouska, J. J., Giranda, V. L., and Greer, J. (2000) Discovering novel ligands for macromolecules using X-ray crystallographic screening, *Nat. Biotechnol.* 18, 1105–1108.
10. Rees, D. C., Congreve, M., Murray, C. W., and Carr, R. (2004) Fragment-based lead discovery, *Nat. Rev. Drug Discovery* 3, 660–672.
11. Shuker, S. B., Hajduk, P. J., Meadows, R. P., and Fesik, S. W. (1996) Discovering high-affinity ligands for proteins: SAR by NMR, *Science* 274, 1531–1534.
12. Bohacek, R. S., McMartin, C., and Guida, W. C. (1996) The art and practice of structure-based drug design: a molecular modeling perspective, *Med. Res. Rev.* 16, 3–50.
13. Fink, T., Bruggesser, H., and Reymond, J.-L. (2005) Virtual exploration of the small-molecule chemical universe below 160 D, *Angew. Chem., Int. Ed.* 44, 1504–1508.
14. Hann, M. M., Leach, A. R., and Harper, G. (2001) Molecular complexity and its impact on the probability of finding leads for drug discovery, *J. Chem. Inf. Comput. Sci.* 41, 856–864.
15. Lu, H., and Tonge, P. J. (2008) Inhibitors of FabI, an enzyme drug target in the bacterial fatty acid biosynthesis pathway, *Acc. Chem. Res.* 41, 11–20.
16. Payne, D. J. (2004) The potential of bacterial fatty acid biosynthetic enzymes as a source of novel antibacterial agents, *Drug News Perspect.* 17, 187–194.
17. Zhang, Y. M., White, S. W., and Rock, C. O. (2006) Inhibiting bacterial fatty acid synthesis, *J. Biol. Chem.* 281, 17541–17544.
18. Miller, J. R., Dunham, S., Mochalkin, I., Banotai, C., Bowman, M., Buist, S., Dunkle, B., Hanna, D., Harwood, H. J., Huband, M. D., Karnovsky, A., Kuhn, M., Limberakis, C., Liu, J. Y., Mehrens, S., Mueller, W. T., Narasimhan, L., Ogden, A., Ohren, J., Prasad, J. V. N. V., Shelly, J. A., Skerlos, L., Sulavik, M., Thomas, V. H., VanderRoest, S., Wang, L., Wang, Z., Whitton, A., Zhu, T., and Stover, C. K. (2009) A class of selective antibacterials derived from a protein kinase inhibitor pharmacophore, *Proc. Natl. Acad. Sci. U.S.A.* 106, 1737–1742.
19. Cronan, J. E., and Waldrop, G. L. (2002) Multi-subunit acetyl-CoA carboxylases, *Prog. Lipid Res.* 41, 407–435.
20. Soriano, A., Radice, A. D., Herbitter, A. H., Langsdorf, E. F., Stafford, J. M., Chan, S., Wang, S., Liu, Y.-H., and Black, T. A. (2006) *Escherichia coli* acetyl-coenzyme A carboxylase: characterization and development of a high-throughput assay, *Anal. Biochem.* 349, 268–276.
21. OpenEye Scientific Software Inc., <http://www.eyesopen.com>.
22. Mochalkin, I., Miller, J. R., Evdokimov, A., Lightle, S., Yan, C., Stover, C. K., and Waldrop, G. L. (2008) Structural evidence for substrate-induced synergism and half-sites reactivity in biotin carboxylase, *Protein Sci.* 17, 1706–1718.
23. Thoden, J. B., Blanchard, C. Z., Holden, H. M., and Waldrop, G. L. (2000) Movement of the biotin carboxylase B-domain as a result of ATP binding, *J. Biol. Chem.* 275, 16183–16190.
24. Tripos, Inc., <http://www.tripos.com>.
25. Schrödinger, LLC., <http://www.schrodinger.com>.
26. Lipinski, C. A., Lombardo, F., Dominy, B. W., and Feeney, P. J. (1997) Experimental and computational approaches to estimate solubility and permeability in drug discovery and development settings, *Adv. Drug Delivery Rev.* 23, 3–25.
27. Hubbard, R. E. (2008) Fragment approaches in structure-based drug discovery, *J. Synchrotron Radiat.* 15, 227–230.
28. Fink, T., and Reymond, J.-L. (2007) Virtual exploration of the chemical universe up to 11 atoms of C, N, O, F: assembly of 26.4 million structures (110.9 million stereoisomers) and analysis for new ring systems, stereochemistry, physicochemical properties, compound classes, and drug discovery, *J. Chem. Inf. Model.* 47, 342–353.
29. Ruud van Deursen, J.-L. R. (2007) Chemical space travel, *ChemMedChem* 2, 636–640.
30. Brinster, S., Lamberet, G., Staels, B., Trieu-Cuot, P., Gruss, A., and Poyart, C. (2009) Type II fatty acid synthesis is not a suitable antibiotic target for Gram-positive pathogens, *Nature* 458, 83–86.
31. Fulmer, T. (2009) Not so FAS, *SciBX* 2, March 19, 2009. DOI: 10.1038/scibx.2009.430.
32. Williams, J. W., and Morrison, J. F. (1979) The kinetics of reversible tight-binding inhibition, in *Methods in Enzymology* (Purich, D. L., Ed.) Vol. 63, pp 437–467, Academic Press, New York.
33. Mayer, M. B., and Meyer, B. (1999) Characterization of ligand binding by saturation transfer difference NMR spectroscopy, *Angew. Chem., Int. Ed.* 38, 1784–1788.
34. Harina, B. M., Bothner-By, A. A., and Gill, T. J. (1977) Nuclear magnetic resonance and fluorescence studies of the binding of O-carboxymethyl-4-methylumbelliferone to its specific antibody, *Biochemistry* 16, 4504–4512.
35. Hwang, T. L., and Shaka, A. J. (1995) Water suppression that works. Excitation sculpting using arbitrary wave-forms and pulsed-field gradients, *J. Magn. Reson., Ser. A* 112, 275–279.
36. Otwinowski, Z., and Minor, W. (1997) Processing of X-ray diffraction data collected in oscillation mode, in *Macromolecular Crystallography: Part A* (Carter, C. W., Jr., and Sweet, R. M., Eds.) pp 307–326, Methods in Enzymology, Vol. 276, Academic Press, San Diego, CA.
37. Vagin, A. A., and Teplyakov, A. (1997) MOLREP: an automated program for molecular replacement, *J. Appl. Crystallogr.* 30, 1022–1025.
38. Brunger, A. T. (1998) Crystallography & NMR system: a new software suite for macromolecular structure determination, *Acta Crystallogr. D* 54 905–921.
39. Murshudov, G. N., Vagin, A. A., and Dodson, E. J. (1997) Refinement of macromolecular structures by the maximum-likelihood method, *Acta Crystallogr. D* 53 240–255.
40. Emsley, P., and Cowtan, K. (2004) Coot: model-building tools for molecular graphics, *Acta Crystallogr. D* 60 2126–2132.
41. Laskowski, R. A., MacArthur, M. W., Moss, D. S., and Thornton, J. M. (1993) PROCHECK: a program to check the stereochemical quality of protein structures, *J. Appl. Crystallogr.* 26, 283–291.
42. Hopkins, A. L., Groom, C. R., and Alex, A. (2004) Ligand efficiency: a useful metric for lead selection, *Drug Discovery Today* 9, 430–431.